

# Diffusion Tensor Image Registration Using Tensor Geometry and Orientation Features

Jinzhong Yang, Dinggang Shen, Christos Davatzikos, and Ragini Verma

Department of Radiology, University of Pennsylvania, Philadelphia, PA, USA 19104

**Abstract.** This paper presents a method for deformable registration of diffusion tensor (DT) images that integrates geometry and orientation features into a hierarchical matching framework. The geometric feature is derived from the structural geometry of diffusion and characterizes the shape of the tensor in terms of prolateness, oblateness, and sphericity of the tensor. Local spatial distributions of the prolate, oblate, and spherical geometry are used to create an attribute vector of geometric feature for matching. The orientation feature improves the matching of the WM fiber tracts by taking into account the statistical information of underlying fiber orientations. This attribute vector is incorporated into a hierarchical deformable registration framework to develop a diffusion tensor image registration algorithm. Extensive experiments on simulated and real brain DT data establish the superiority of the features for deformable matching of diffusion tensors, thereby aiding in atlas creation. The robustness of the method makes it potentially useful for group-based analysis of DT images acquired in large studies to identify disease-induced and developmental changes.

**Keywords:** Diffusion tensor imaging, structural geometry, tensor orientation, attribute vector, deformable registration.

## 1 Introduction

Diffusion tensor imaging (DTI) has emerged as a powerful and effective technique for analyzing the underlying white matter structure of brains [1]. DTI provides unique micro-structural and physiological insight into white matter tissue of brains, which in turn facilitates the study of development, aging, and disease on specific white matter regions of interest. In order to carry out group-based analysis and statistics, it is imperative to make different subjects comparable, thus requiring the spatial normalization of diffusion tensor (DT) images. However, spatial normalization of DT images is rendered challenging by the fact that the data representation is high dimensional and it requires not only the spatial warping, but also the tensor reorientation at each voxel [2, 3]. Recent advances in DT image normalization either employed a combination of different scalar maps derived from full tensor image for a multi-channel registration [4], or developed registration algorithms based on the full tensor similarity measurements [5, 6]. However, the normalization based on features extracted from full tensors has not been extensively researched yet. An earlier study applied oriented 3-D Gabor features extracted from tensors for matching [7], while a recent method employed major fiber bundles to align tensors[8]. Both methods demonstrate that registration accuracy

can be improved and better correspondence can be obtained in the white matter if features that characterize both tensor shape and orientation are used for matching with carefully chosen metrics.

In this paper, we design a feature vector that incorporates tensor geometry and orientation features for DTI registration. We capitalize on the structural geometry of the diffusion tensor [9] and develop a novel attribute vector consisting of geometric moments computed from the local spatial histograms of tensor geometric measures. In order to improve the registration accuracy of white matter (WM) fiber tracts, we also incorporate the local statistical information of underlying fiber orientations into the attribute vector. This attribute vector is rotationally invariant, and integrates spatial information from local histograms computed at different scales. We include this attribute vector into a hierarchical deformable registration technique on the lines of [10], to develop a deformable registration method for diffusion tensor images. Extensive experiments demonstrate the robustness and accuracy of DT image registration using the proposed feature vector.

## 2 Methods

Let  $\lambda_1 \geq \lambda_2 \geq \lambda_3 \geq 0$  be the three eigenvalues of a symmetric tensor  $\mathbf{D}$ , and  $\hat{\mathbf{e}}_i$  be the normalized eigenvector corresponding to  $\lambda_i$ , then the tensor  $\mathbf{D}$  can be denoted by

$$\mathbf{D} = \lambda_1 \hat{\mathbf{e}}_1 \hat{\mathbf{e}}_1^T + \lambda_2 \hat{\mathbf{e}}_2 \hat{\mathbf{e}}_2^T + \lambda_3 \hat{\mathbf{e}}_3 \hat{\mathbf{e}}_3^T. \quad (1)$$

Geometrically, tensor  $\mathbf{D}$  can be represented by an ellipsoid with three axes oriented along its three eigenvectors, and three semi-axis lengths proportional to the square root of its three eigenvalues. Different shapes of the ellipsoid give rise to three geometric structures of diffusion tensors: prolate (linear) structure, in which diffusion is mainly in the direction corresponding to  $\hat{\mathbf{e}}_1$ ; oblate (planar) structure, in which diffusion is restricted to a plane spanned by  $\hat{\mathbf{e}}_1$  and  $\hat{\mathbf{e}}_2$ ; and spherical structure with isotropic diffusion. Three geometric measures were proposed in [9] to describe how close the diffusion tensor is to the generic structures of prolateness, oblateness, and sphericity. They are respectively defined as

$$c_l = \frac{\lambda_1 - \lambda_2}{\lambda_1}, c_p = \frac{\lambda_2 - \lambda_3}{\lambda_1}, c_s = \frac{\lambda_3}{\lambda_1}. \quad (2)$$

### 2.1 Tensor geometric feature for matching

A discriminative attribute vector is defined at each voxel from the geometric measures in (2). This attribute vector characterizes the local diffusion property by combining the local distributions of prolate, oblate, and spherical structures. For a specified voxel  $v$ , local histograms  $\mathbf{h}_l(v)$  of  $c_l$ ,  $\mathbf{h}_p(v)$  of  $c_p$ , and  $\mathbf{h}_s(v)$  of  $c_s$  are computed from a spherical neighborhood region of voxel  $v$  with a given appropriate radius  $r$ . These

histograms roughly characterize the distribution of the tensor geometry in the neighborhood region. For each histogram, we compute its regular geometric moments as the statistical geometric features, i.e.

$$m_k(v, n) = \sum_i i^n \mathbf{h}_k(v, i), \quad k = l, p, s; \quad (3)$$

where  $\mathbf{h}_k(v, i)$  is the frequency of index  $i$  in histogram  $\mathbf{h}_k(v)$ , and  $m_k(v, n)$  is the  $n$ th order moment of this histogram. Low-order geometric moments are used to represent the geometric features for a histogram and form a vector as

$$\mathbf{a}_k^{hist}(v) = \{m_k(v, n) \mid n = 0, 1, 2\}, \quad k = l, p, s. \quad (4)$$

In order to improve the accuracy of matching, we include the boundary attribute  $b_{FA}^{bound}(v)$  of fractional anisotropy (FA) and the boundary attribute  $b_{ADC}^{bound}(v)$  of apparent diffusion coefficient (ADC) into the attribute vector. These boundary attributes are computed by a Canny edge detector [11] from FA and ADC scalar maps of DT image respectively. Therefore, the complete attribute vector at voxel  $v$  can be represented as

$$\mathbf{a}(v) = [\mathbf{a}_l^{hist}(v), \mathbf{a}_p^{hist}(v), \mathbf{a}_s^{hist}(v), b_{FA}^{bound}(v), b_{ADC}^{bound}(v)]. \quad (5)$$

Since the histograms for computing the geometric features are generated from a spherical region, they are invariant to a rotational transformation. Therefore, the attribute vector defined in (5) is rotationally invariant, which makes it attractive for registration. To make the feature vector more discriminative, the above attribute vector is computed at three different scales so that both global and local geometric features are accounted for. In each scale, the similarity of two attribute vectors,  $\mathbf{a}(u)$  and  $\mathbf{a}(v)$ , of two points,  $u$  and  $v$ , is defined as

$$m(\mathbf{a}(u), \mathbf{a}(v)) = \prod_i (1 - |\mathbf{a}_i(u) - \mathbf{a}_i(v)|), \quad (6)$$

where  $\mathbf{a}_i(\cdot)$  is the  $i$ th element in the attribute vector.

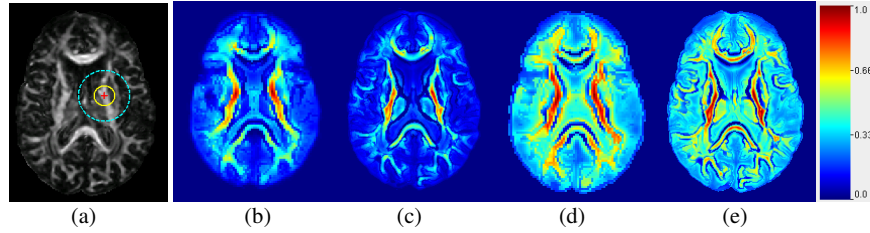


**Fig. 1.** Similarity of the points on major fiber tracts. The attribute vector of the crossed point in (a) is compared with the attribute vectors of other points in the image. (b) and (c) show the resulting map of similarities using the geometric feature computed at a coarse scale and a fine scale, respectively. (d) and (e) show the resulting map of similarities using the FA feature computed at a coarse scale and a fine scale, respectively. Red indicates high similarity.

We demonstrate the discriminatory power of the proposed attribute vector of geometric feature in Figs. 1 and 2 by comparing it with the FA feature [10] for diffusion

tensor matching. Both points in major fiber tracts and small tracts have been examined. From the color-coded maps of similarities illustrated in Figs. 1 and 2, we can conclude that the geometric feature is much more discriminative than just using FA feature on both major and small fiber tracts (even on a single scale), with geometric feature being far superior on the smaller tracts.

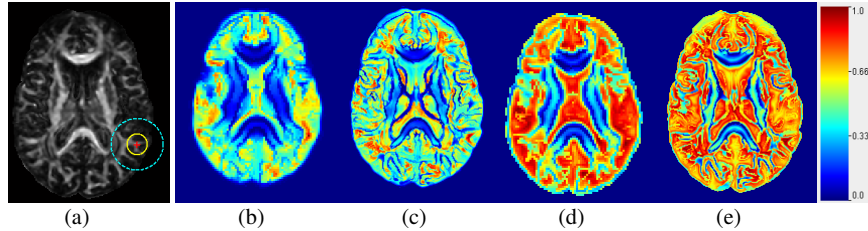


**Fig. 2.** Similarity of the points on small fiber tracts. Legends are the same as those in **Fig. 1**.

## 2.2 Fiber orientation feature for matching

Properly aligning WM fiber tracts is a major concern in DTI registration. In order to further improve the registration accuracy of WM fiber tracts, we incorporate the local statistical information of underlying fiber orientations into the attribute vector defined in (5). The fiber orientation at voxel  $v$  is approximated by the principal direction (PD) of tensor  $\mathbf{D}$  weighted by the FA value at this voxel. Local spatial distribution of PD in the 3D space at voxel  $v$ , denoted by  $\mathbf{H}_{PD}(v)$ , can be estimated from the samples in a spherical neighborhood region with a radius  $r$ . Therefore, the similarity of two points,  $u$  and  $v$ , in terms of local PD distribution can be defined as the normalized mutual information (NMI) of  $\mathbf{H}_{PD}(u)$  and  $\mathbf{H}_{PD}(v)$  as

$$NMI_{PD}(u, v) = 2 - 2 \frac{E[\mathbf{H}_{PD}(u), \mathbf{H}_{PD}(v)]}{E[\mathbf{H}_{PD}(u)] + E[\mathbf{H}_{PD}(v)]}, \quad (7)$$

where  $E$  denotes the joint or marginal differential entropy of the random variables of local PD distribution. The similarity of the attribute vectors with the orientation features at points  $u$  and  $v$  is then determined by the combination of Eqs. (6) and (7) as

$$M(u, v) = m(\mathbf{a}(u), \mathbf{a}(v)) \cdot NMI_{PD}(u, v). \quad (8)$$

$M(u, v)$  ranges from 0 to 1 where 1 indicates the most similar attribute vectors.

This new attribute vector including the orientation feature serves to further refine the matching of WM fiber tracts after the diffusion tensors are initially registered and reoriented using only the geometric feature. Since the PD of a tensor is meaningful only in the high anisotropic anatomies such as WM fiber tracts, we consider the orientation feature only for those points with a high FA value.

### 2.3 Deformable registration with geometry and orientation features

The attribute vector described above is used in conjunction with the deformable techniques on the lines of the HAMMER algorithm [10] to develop a DTI registration algorithm. This algorithm employs a hierarchical structure to select distinct attribute vectors, thus reducing ambiguity in finding correspondences. The boundary attributes of FA and ADC maps are the criterion for choosing active points to drive the registration. In the initial stages of the matching procedure, only a few points with distinct boundary attributes are selected for matching in order to avoid local minima. As the matching progresses, more and more points with lower boundary strengths become reliable and thus are selected to drive the registration. The final spatial transformation is generated by concatenating the hierarchical sequence of piecewise smooth transformations obtained at each stage. The deformation field obtained as part of this spatial warping is used to determine the tensor reorientation, based on a spatially adaptive procedure that estimates the underlying fiber orientation [2], to produce properly oriented tensors in the atlas space.

## 3 Results

We have demonstrated the high matching accuracy of the geometric feature in different parts of the white matter fiber tracts in Figs. 1 and 2. In this section, we applied our method to register both human brains and mouse brains to demonstrate the efficiency of our method by comparing with two alternative deformable registration algorithms, HAMMER [10] and Demons algorithm [12] when applied to FA maps. For the sake of simplicity and fairness, we compare FA feature-based registration with the geometric feature, establishing the superiority of the latter. In the next stage we also demonstrate that the orientation feature together with the geometric feature improves the matching of the WM fiber tracts.

### 3.1 Matching accuracy comparison: geometric feature and FA feature

Ten simulated human brain DT images are generated by applying ten simulated deformation fields [13] to warp a template DT image. These ten simulated DT images are then registered back to the template space by using the attribute vector of geometric feature and FA feature, respectively. The deformation errors between the registration results and the simulated ground truth are calculated for both features. Fig. 3 shows the average registration error and the variance in each subject computed from the whole brain and WM fiber tracts, respectively. It demonstrates that using the geometric feature yields more accurate registration than using the FA feature, with respective population means as 0.89 voxels and 1.11 voxels for the whole brain. Comparing Figs. 3(a) and (b) shows the registration to be superior in the WM fiber tracts. The respective population means using geometric feature and FA feature are 0.75 voxels and 0.93 voxels in the regions with  $FA > 0.25$ .

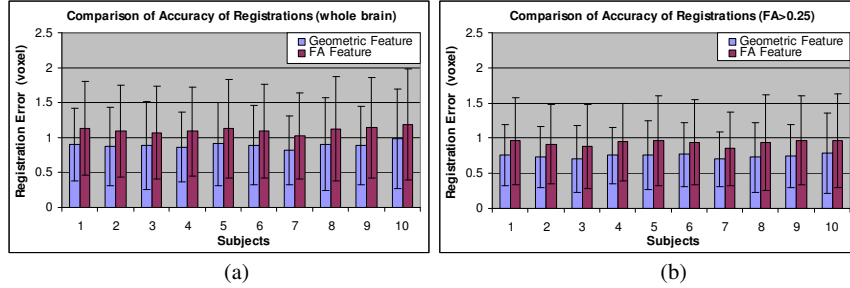


**Fig. 3.** Comparison of the registration accuracy using the geometric feature and FA feature. (a) shows the registration error computed from the whole brain, and (b) shows the registration error computed from WM fiber tracts with FA > 0.25.

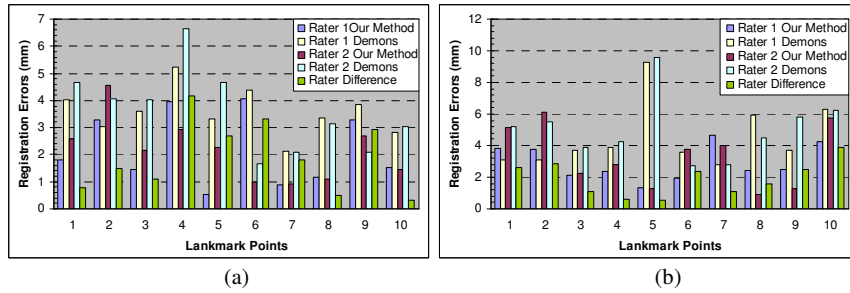


**Fig. 4.** Comparison of the registration errors on each of 10 landmark points identified by two raters on both major and minor WM fiber tracts, in two subjects (a) and (b), respectively.

### 3.2 DTI registration of human brains

To further demonstrate the efficiency of our method, we apply it to register real human brain DT images and compare it with the demons algorithm, which is implemented with ITK [14] and is applied to FA images. The same tensor reorientation scheme [2] is applied together with demons registration to produce the final warped DT image. Two subjects were registered to a template, each with voxel resolution as  $0.9375 \times 0.9375 \times 2.5$  mm. We had two raters pick up 10 corresponding landmarks from each subject and template. These landmarks reside in both major and minor WM fibers and serve to evaluate the matching accuracy. For each pair of corresponding landmarks, we compute the registration errors for our proposed method and the demons algorithm. These results are shown in Fig. 4. We also show the variation between two raters for better understanding. Fig 4 shows that overall our method achieves more accurate and robust registration than the demons algorithm does. To visually observe the registration of WM fiber tracts, we demonstrate the overlaid WM fiber tracts in Fig 5. In Fig. 5, we compare the registered fiber tracts obtained from the demons algorithm, our method without adding the orientation feature described in Section 2.2, and our method with the added orientation feature. The results show that

the registration with the orientation feature achieves the best matching of WM fiber tracts.

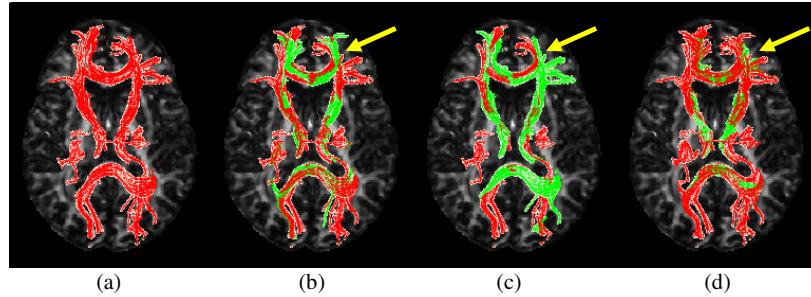


**Fig. 5.** Comparison of the overlaid WM fiber tracts in 3D space. (a) shows the WM fiber tracts extracted from the template. (b), (c), and (d) show the overlaid fiber tracts extracted from registered DT images by the demons algorithm, our method without adding orientation feature, and our method with added orientation feature, respectively.

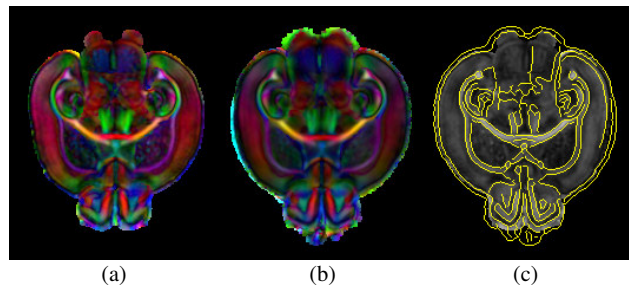


**Fig. 6.** Spatial normalization of 5 mouse brains. (a) Color map of the template. (b) Color map of the group averaged image. (c) Edges extracted from FA map of group averaged image superimposed on the FA map of template.

### 3.3 Creating an atlas of murine brains

We apply our method to spatially normalize 5 mouse brains scanned at Day 10 in order to create an atlas for this development stage by group-averaging the normalized DT images. One subject is identified as the template and the others are registered to it using the proposed method. The group-averaged image is computed by voxel-wise averaging the corresponding tensors in the individual warped subjects. Fig. 6 visually demonstrates the registration accuracy. The color map in Fig. 6 is the tensor PD weighted by the corresponding FA value. The color is encoded with green representing anterior-posterior, blue for feet-head, and red for left-right orientation. The sharpness of the average in Fig. 6(b) as compared to the template in Fig. 6(a), as well as the good matching of the edge map to the underlying FA image in Fig. 6(c), shows that a good spatial normalization has been achieved and even the thin tracts like internal and external capsules have been aligned well.

## 4 Conclusions

In conclusion, we have presented a novel attribute vector that characterizes the geometry and orientation of diffusion tensors and hence obtains superior matching and subsequent deformable registration. The features are incorporated into a hierarchical deformable registration algorithm, and the orientation feature improves the matching of the WM fiber tracts. The extensive experiments verified the efficiency of the features for matching of tensors and subsequently in obtaining a fully deformable registration framework for diffusion tensor images.

## References

1. Pierpaoli, C., Jezzard, P., Basser, P. J., Barnett, A., and Chiro, G. D.: Diffusion tensor MR imaging of human brain. *Radiology*. 201(3), 637-648 (1996)
2. Xu, D., Mori, S., Shen, D., Zijl, P. C. M. v., and Davatzikos, C.: Spatial Normalization of Diffusion Tensor Fields. *Magnetic Resonance in Medicine*. 50(1), 175-182 (2003)
3. Alexander, D. C., Pierpaoli, C., Basser, P. J., and Gee, J. C.: Spatial transformations of diffusion tensor magnetic resonance images. *IEEE Transactions on Medical Imaging*. 20(11), 1131-1139 (2001)
4. Park, H. J., Kubicki, M., Shenton, M. E., Guimond, A., McCarley, R. W., Maier, S. E., Kikinis, R., Jolesz, F. A., and Westin, C.-F.: Spatial Normalization of Diffusion Tensor MRI Using Multiple Channels. *Neuroimage*. 20(4), 1995-2009 (2003)
5. Cao, Y., Miller, M., Mori, S., Winslow, R. L., and Younes, L.: Diffeomorphic matching of diffusion tensor images. In: *MMBIA*, pp. 67. New York, NY (2006)
6. Zhang, H., Yushkevich, P. A., Alexander, D. C., and Gee, J. C.: Deformable registration of diffusion tensor MR images with explicit orientation optimization. *Medical Image Analysis*. 10(5), 764-785 (2006)
7. Verma, R. and Davatzikos, C.: Matching of Diffusion Tensor Images Using Gabor Features. In: *Proceedings of the IEEE International Symposium on Biomedical Imaging (ISBI)*, pp. 396-399. Arlington, Va. (2004)
8. Ziyang, U., Sabuncu, M. R., O'Donnell, L. J., and Westin, C.-F.: Nonlinear Registration of Diffusion MR Images Based on Fiber Bundles. In: *MICCAI*, pp. 351-358. (2007)
9. Westin, C.-F., Maier, S. E., Mamata, H., Nabavi, A., Jolesz, F. A., and Kikinis, R.: Processing and Visualization of Diffusion Tensor MRI. *Medical Image Analysis*. 6, 93-108 (2002)
10. Shen, D.: Image Registration by Local Histogram Matching. *Pattern Recognition*. 40, 1161-1171 (2007)
11. Canny, J.: A computational approach to edge detection. *IEEE Transactions on Pattern Analysis and Machine Intelligence*. 8(6), 679-698 (1986)
12. Thirion, J. P.: Non-rigid matching using demons. In: *Proceedings of IEEE Conference on Computer Vision and Pattern Recognition*, pp. 245-251. (1996)
13. Xue, Z., Shen, D., Karacali, B., Stern, J., Rottenberg, D., and Davatzikos, C.: Simulating deformations of MR brain images for validation of atlas-based segmentation and registration algorithms. *NeuroImage*. 33(3), 855-866 (2006)
14. ITK Software Guide, <http://www.itk.org/HTML/Documentation.htm>